# HHS Public Access

Author manuscript

*Stem Cells*. Author manuscript; available in PMC 2017 April 01.

# Role of Acid Sphingomyelinase in Shifting the Balance Between Proinflammatory and Reparative Bone Marrow Cells in Diabetic Retinopathy

**Harshini Chakravarthy**[a], **Svetlana Navitskaya**[a], **Sandra O'reilly**[a], **Jacob Gallimore**[b], **Hannah Mize**[b], **Eleni Beli**[c], **Qi Wang**[a], **Nermin Kady**[a], **Chao Huang**[a], **Gary J. Blanchard**[b], **Maria B. Grant**[c], and **Julia V. Busika**[a]

[a]Department of Physiology Michigan State University, East Lansing, Michigan, USA

[b]Department of Chemistry, Michigan State University, East Lansing, Michigan, USA

[c]Department of Ophthalmology, Indiana University School of Medicine, Indianapolis, Indiana, USA

## Abstract

The metabolic insults associated with diabetes lead to low-grade chronic inflammation, retinal endothelial cell damage, and inadequate vascular repair. This is partly due to the increased activation of bone marrow (BM)-derived proinflammatory monocytes infiltrating the retina, and the compromised function of BM-derived reparative circulating angiogenic cells (CACs), which home to sites of endothelial injury and foster vascular repair. We now propose that a metabolic link leading to activated monocytes and dysfunctional CACs in diabetes involves upregulation of a central enzyme of sphingolipid signaling, acid sphingomyelinase (ASM). Selective inhibition of ASM in the BM prevented diabetes-induced activation of BM-derived microglia-like cells and normalized proinflammatory cytokine levels in the retina. ASM upregulation in diabetic CACs caused accumulation of ceramide on their cell membrane, thereby reducing membrane fluidity and impairing CAC migration. Replacing sphingomyelin with ceramide in synthetic membrane vesicles caused a similar decrease in membrane fluidity. Inhibition of ASM in diabetic CACs improved membrane fluidity and homing of these cells to damaged retinal vessels. Collectively, these findings indicate that selective modulation of sphingolipid metabolism in BM-derived cell populations in diabetes normalizes the reparative/proinflammatory cell balance and can be explored as a novel therapeutic strategy for treating diabetic retinopathy.

## Keywords

Diabetic retinopathy; Bone marrow transplantation; Sphingolipids; Dyslipidemias; Vascular system injuries

Correspondence: Julia V. Busik, Ph.D., 3178 Biomedical Physical, Science Building, East Lansing, Michigan 48824, USA., Telephone: 517-884-5118; Fax: 517-355-5125; busik@msu.edu.

**DISCLOSURE OF POTENTIAL CONFLICT OF INTEREST** The authors indicate no potential conflicts of interest.

## Introduction

Diabetic retinopathy (DR) is a sight-threatening complication of diabetes. Available DR treatment options are highly invasive and only help to slow progression of the disease. Hyperglycemia and dyslipidemia are major metabolic abnormalities in diabetes. Molecular pathogenesis of hyperglycemia and dyslipidemia-induced damage to the retina is not clear but may involve several mechanisms including oxidative stress, activation of protein kinase C, accumulation of polyols, and advanced glycation end-products, endoplasmic reticulum (ER) stress, and chronic low-grade inflammation [1, 2]. Although clinical manifestations of DR are due to vascular abnormalities including increased microvascular permeability, vessel leakage, microaneurysms formation, and eventually capillary drop-out, and pathological neovascularization [1], recent studies demonstrated that most retinal cell types contribute to pathogenesis of the disease. Activated retinal glial cells and pigment epithelial cells in diabetes express proinflammatory cytokines and vascular endothelial growth factor (VEGF), contributing to damage of endothelial cells lining the retinal vasculature [3–5]. Impaired retinal insulin receptor signaling contributes to metabolic stress to neurons, which may in turn impair blood-retinal barrier integrity [6].

In addition to direct effects on the retina, hyperglycemia and dyslipidemia can indirectly affect the retina through the induction of bone marrow (BM) pathology. Hematopoietic stem cells (HSC) in the BM give rise to lymphoid and myeloid progenitors that differentiate into blood cells. BM pathology in diabetes is proposed to cause activation of circulating myelomonocytic cells, leading to increased leukocyte adhesion, which contributes to retinal inflammation [6, 7]. Several studies have found that myeloid-derived monocytes can infiltrate the diabetic retina, adopt a microglia-like phenotype, and exacerbate inflammation by secreting proinflammatory cytokines. This cytokine secretion can further activate resident microglia, astrocytes, and Müller glia in the retina [5, 8, 9].

We have previously demonstrated that, in addition to increase in proinflammatory leukocytes, diabetes induces a reduction of vascular reparative cells [10, 11]. Circulating angiogenic cells (CACs) are BM-derived vascular reparative cells known to be exquisitely sensitive to the diabetic milieu [12–14]. Release of CACs from BM into circulation and extravasation into tissues is a critical component of their physiological role as reparative cells. Indeed, there is growing interest in understanding stem/progenitor cell migration and developing interventions that increase homing efficiency of CACs to sites of tissue damage [14–17]. Recent studies indicate that CACs isolated from diabetic individuals are ineffective at vascular regeneration due to reduced migratory and proliferation abilities [12, 14, 15]. We recently demonstrated that reduced deformability of human CACs in diabetes is linked to decrease in migratory prowess of these cells [14]. Thus, modulating cell deformability can provide a way of improving mobilization efficiency of CACs to sites of vascular injury.

The individual molecular steps causing retinal inflammation and impaired vascular repair are not well-understood but probably involve hyperglycemia and dyslipidemia associated with diabetes. Clinical studies have demonstrated strong associations between dyslipidemia and development of DR [18, 19]. Bioactive sphingolipid metabolites like ceramide, glycosphingolipids, and sphingosine 1-phosphate (S1P) are believed to play crucial roles in

development of DR [20–24]. Acid sphingomyelinase (ASM), the enzyme converting sphingomyelin to ceramide, is a key element activated by diabetes in both CACs and retinal vasculature. We have previously shown that ASM is important for cytokine signaling in retinal endothelial cells, and that inhibition of ASM prevents retinal inflammation and vascular degeneration associated with diabetes [13, 20, 25]. In this report, we describe a link between increased ASM activity in the BM cells and shift in BM-derived inflammatory and reparative cell function in the diabetic retina.

## Materials and Methods

### Mice

All procedures involving animal models were approved by Institutional Animal Care and Use Committee at MSU. Male C57BL/6J and C57BL/6-Tg(CAG-EGFP) mice were purchased from Jackson Laboratory (Bar Harbor, ME, http://www.jax.org) and made diabetic by injections of 55 mg streptozotocin (STZ) (Sigma Aldrich, St. Louis, http://www.sigmaaldrich.com) per kg body weight for five consecutive days. Insulin (0–2 units per day) was administered to prevent acute weight loss, while maintaining hyperglycemia (~20 mmol/L blood glucose).

### Generation of ASM$^{-/-}$, ASM$^{-/-}$ × gfp$^+$, and gfp$^+$ Chimeras

ASM$^{-/-}$ mice used as donor strain were obtained from Dr. Kolesnick (with permission of Dr. Schuchman), and C57BL/6-Tg(CAG-EGFP) transgenic donor strain from Jackson Laboratory. C57BL/6.ASM$^{-/-}$, C57BL/6.gfp$^+$, and C57BL/6.ASM$^{-/-}$ × gfp$^+$ chimeras were generated by irradiating recipient 8-weeks old C57BL/6 mice with 1,100 rads followed by retroorbital injection of BM ($2 \times 10^6$ cells) from donor mice. Wild-type (WT) BM donor cells transferred into WT recipient chimeras were used as control.

### Retinal Vascular Permeability

In vivo retinal vascular permeability was assessed after tail vein injections of fluorescein isothiocyanate (FITC)-labeled albumin 20 mg/kg (Sigma-Aldrich), as described previously [26]. Images of flat-mounted retinas were captured using Olympus FluoView 1000 Laser Scanning confocal microscope. Retinas were disrupted mechanically and cleared by centrifugation. FITC-albumin in supernatant was quantified using spectrofluorometer and normalized to plasma fluorescence.

### Acellular Capillaries

Mice eyes were enucleated, and retinal vasculature was isolated by elastase digestion [20]. Retinal vasculature was stained with hematoxylin and eosin. Acellular capillaries in midretina were systematically counted by three investigators as described previously [20]. All samples were analyzed in a masked manner.

### Quantitative Real-Time Polymerase Chain Reaction

Total RNA was extracted from mice retinas and quantitative reverse transcriptase polymerase chain reaction (RT-PCR) was performed as described previously [20]. Mouse

gene-specific primers for ASM, intercellular adhesion molecule (ICAM-1), vascular cell adhesion molecule (VCAM-1), VEGF A, and interleukin 1β (IL-1β) were used. All results were normalized to cyclophilin.

### Western Blot Analysis

Protein extraction and Western blot analysis were performed as previously described [20]. Anti-ASM primary antibody (Cell Signaling Technology, Beverly, MA, http://www.cellsignal.com, 1:1,000 dilution) followed by Alexa-Fluor secondary antibody (Life Technologies, Rockville, MD, http://www.lifetech.com) were used.

### CAC Isolation and Migration

Mice were euthanized, tibias and femurs collected, flushed with ice-cold phosphate buffered saline (PBS) and made into single cell suspension. Cells were treated with ammonium chloride (Stem Cell Technologies, Vancouver, BC, Canada, http://www.stemcell.com) to remove erythrocytes and enriched for mouse hematopoietic stem/progenitor cells using negative selection kit, followed by Sca-1 positive selection (Stem Cell Technologies) to obtain $Lin^-$ $Sca-1^+$ progenitor cells. Cells were maintained overnight at 37°C in 5% $CO_2$ in humidified cell culture incubator, in endothelial cell growth medium (EGM-2) media with SingleQuot supplements and growth factors (Lonza, Allendale, NJ, USA, http://www.lonza.com/). Cells were stained with Calcein-AM (BD Biosciences, San Diego, http://www.bdbiosciences.com) and migration assay performed as described previously [13]. The cells isolated by this protocol were formerly called EPCs (endothelial progenitor cells). The terminology has now been updated to CACs, which is more reflective of the function of these cells [27].

### Unilamellar Vesicle Formation

Unilamellar vesicles were formed by extrusion. Batch 1 was composed of 49 mol% dioleoyl phosphatidylcholine (DOPC), 1 mol% perylene, 10 mol% cholesterol, and 40 mol% sphingomyelin (chicken egg), and batch 2 of 49 mol% DOPC, 1 mol% perylene, 10 mol% cholesterol, 20 mol% sphingomyelin, 20 mol% ceramide. Perylene was purchased from Sigma Aldrich and other vesicle constituents from Avanti Polar Lipids (Alabaster, AL, USA http://www.avantilipids.com/). Constituents were present in chloroform or ethanol (perylene), aliquots were evaporated to dryness and taken up in 2.86 mL milli-Q water. The mixture was put through five freeze-thaw-vortex cycles and extruded 11 times through a polycarbonate filter [28]. The extruded vesicles were measured by DLS and were approximately 200 nm in diameter.

### Membrane Fluidity Measurements

10,000 CACs were labeled with perylene [28] (10μM) for 15 minutes. Polarized fluorescence measurements were collected using time-correlated single-photon counting instrument, as described previously [28]. The instrument response function is approximately 35 ps fwhm. Perylene emission transients (470 nm) were collected for polarizations parallel ($I_{II}(t)$) and perpendicular ($I_\perp(t)$) to vertically polarized excitation pulse (435 nm). The polarized emission transients are used to construct the induced orientational anisotropy

decay function, $r(t)$, which decays with a single exponential functionality and time constant of decay, $\tau_{OR}$, is given by the modified Debye-Stokes-Einstein equation,

$$r(t) = \frac{I_{\parallel}(t) - I_{\perp}(t)}{I_{\parallel}(t) - 2I_{\perp}(t)} = r(0) \quad \exp \quad (-t/\tau_{OR})$$

$$\tau_{OR} = \frac{\eta V f}{k_B T S}$$

where $\eta$ is viscosity of the medium, $V$ is hydrodynamic volume of perylene (225 Å$^3$), $k_B T$ is a thermal energy term, $f$ and $S$ are constants to account for frictional interactions between perylene and its surroundings, and the nonspherical shape of perylene. For all measurements, $V$, $f$, $S$, and $T$ remain constant and changes in $\tau_{OR}$ reflect changes in $\eta$.

## ASM Gene Inhibition

CACs were resuspended in electroporation solution (Lonza) to final concentration of $5 \times 10^5$ cells per 100 μL, mixed with 300 nM ASM small interfering RNA (siRNA), and electroporated (Nucleofector program M-030, Lonza). Cells were maintained in supplemented medium at 37°C in 5% $CO_2$ in humidified incubator for 48 hours. Approximately fivefold inhibition of ASM expression was obtained as determined by RT-PCR and Western Blot.

## Reendothelialization of Retinal Vasculature

10,000 Lin$^-$Sca$^+$gfp$^+$ progenitor cells were injected intravitreously using 33-gauge (Hamilton Company, Reno, NV, USA, http://www.hamiltoncompany.com/), into diabetic and control WT mice. After 7 days to allow progenitor cells homing to retinal vessels, mice were sacrificed, eyes removed, pierced with a 30-gauge needle, fixed in 4% paraformaldehyde for 1 hour, and washed in PBS. Retinas were isolated and permeabilized overnight at 4°C in HEPES-buffered saline containing 0.1% Tween 20 and 1% bovine serum albumin (BSA). Vasculature was stained with rabbit anti-collagen IV (Abcam, Cambridge, U.K., http://www.abcam.com) diluted 1:400, followed by PBS wash. Secondary antibody chicken anti-rabbit (Alexa Fluor 594, Invitrogen, Carlsbad, CA, http://www.invitrogen.com), diluted 1:1,000 was used.

## Immunofluorescent Staining

**Ceramide in BM Cells**—CACs were treated with anticeramide (Sigma Aldrich) antibody and corresponding secondary antibody (Thermo Fisher Scientific, Waltham, MA, USA, https://www.thermofisher.com).

**Microglia in the Retina**—Retinal flat-mounts from gfp$^+$ chimeras were stained for microglia using 1:100 diluted goat anti-Iba-1 (Novus Biologicals, Littleton, CO, USA, http://www.novusbio.com/). BM-derived microglia cells were defined by gfp$^+$, Iba-1$^+$ staining and shape. Mean counts of Iba$^+$ gfp$^+$ cells were taken from three points within central retina at

×20 magnification. Length of primary dendrites of microglia was quantified using MetaMorph software. All measurements were done in a masked fashion. Nikon TE2000 fluorescence microscope with Photometrics CoolSNAP HQ2 camera was used for imaging. Staining was quantified using MetaMorph software (Molecular Devices, Downingtown, PA, http://www.moleculardevices.com).

### Transferase-Mediated Deoxyuridine Triphosphate (dUTP) Nick-End Labeling Staining

TACS-XL Basic In Situ Apoptosis Detection Kit (https://www.trevigen.com) was used on paraffin-embedded sections according to manufacturer's protocol. Number of terminal deoxynucleotidyl transferase dUTP nick end labeling (TUNEL)-positive cells in ganglion cell layer (GCL), inner nuclear layer (INL), and outer nuclear layer (ONL) were counted, and data expressed per retina [20].

### Morphometric Analysis

Retinal sections were stained with hematoxylin and eosin, and thickness of inner plexiform layer (IPL), INL, outer plexiform layer (OPL), and ONL was measured using images captured from four microscopic fields with Nikon TE2000 microscope and color camera. Calibrated lines were drawn perpendicular to each layer of the retina using Metamorph software, and average thickness of each retinal layer was expressed in μm.

### Flow Cytometry

Flow cytometry was performed using LSR II instrument (BD Biosciences). Data were analyzed with FlowJo software (Tree Star, Oregon, USA, http://www.treestar.com/). Antibodies were purchased from eBioscience, San Diego, CA, USA, http://www.ebioscience.com/.

### Mass Spectrometry

One to five million cells were subjected to monophasic lipid extraction. High resolution mass spectra were acquired using a Thermo Scientific model LTQ Orbitrap Velos mass spectrometer (San Jose, CA, http://www.thermoscientific.com/) and Advion Triversa Nanomate nESI source (Advion, Ithaca, NY, http://www.advion.com/) as previously described [29].

### Statistical Analyses

Data are presented as mean±SEM. Results were analyzed for statistical significance by Student's *t* test or one-way ANOVA followed by Tukey's or Bonferroni's post hoc test (GraphPad Prism5, GraphPad Software, San Diego, CA http://www.graphpad.com/), where appropriate.

## Results

### ASM-Deficiency in BM Prevents Inflammation in Diabetic Retina

To address the specific role of ASM in affecting BM cells, C57BL/6J mice were transplanted with ASM$^{-/-}$, ASM$^{-/-}$×gfp$^+$, or WT age-matched BM. After 4 months to allow

stable reconstitution, mice were made diabetic with STZ injections. Table 1 shows body weights and blood glucose levels for diabetic and control chimeras. By 2 weeks after onset of diabetes, diabetic mice weighed significantly less and their blood glucose levels were significantly higher than control mice. ASM$^{-/-}$ → WT and WT → WT BM transplanted (BMT) diabetic mice had similar degree of diabetes throughout the study (Table 1).

Previous studies showed that diabetes causes accumulation of BM-derived monocytes in the retina. These monocytes adopt a microglia-like phenotype and contribute to retinal inflammation by secreting proinflammatory cytokines [5, 8, 9]. Microglial activation is usually identified by morphological changes, involving retraction of highly ramified processes and assuming amoeboid shape with thicker dendrites and larger cell bodies [30–32]. We anticipated that ASM$^{-/-}$ phenotype in the diabetic BM may influence activation of BM-derived microglia-like population. To distinguish cells migrating to the retina from the BM, retinas from gfp$^+$·WT and ASM$^{-/-}$×gfp$^+$·WT BM chimeras were examined after 3 months of diabetes. Although no significant difference in numbers of BM-derived microglia-like cells was observed in chimeric mice, more activation of BM-derived gfp$^+$ microglia was seen in retinas of diabetic gfp$^+$·WT BM chimeras. ASM$^{-/-}$×gfp$^+$·WT BMT prevented this increase in microglial activation in diabetic retinas (Fig. 1A), indicating that ASM upregulation in these cells may contribute to inflammation in the diabetic retina.

The pathogenesis of DR involves chronic low-grade inflammation, and studies show that activated glial cells may contribute to cytokine production in the diabetic retina [2, 30–32]. The twofold or less changes in inflammatory markers in the diabetic retina reported here are consistent with low-grade inflammation associated with DR [5]. ASM deficiency in BM prevented diabetes-associated upregulation of inflammatory markers and growth factors like IL-1β, VEGF, ASM, ICAM-1, and VCAM-1 in retina of chimeric mice after 2 months of diabetes (Fig. 1B).

In order to visualize retinal neuronal changes, we measured the thickness of the inner retinal layers and performed TUNEL staining of retinal sections. No gross differences in retinal structure and inner retinal thickness were observed in control, diabetic, and diabetic mice with ASM$^{-/-}$ BM at 8 weeks of diabetes, in agreement with a previous study [33]. The number of apoptotic neurons detected by TUNEL-positive cells was also similar in all groups (Supporting Information Fig. S1), which is in agreement with Feit-Leichman et al. showing that neuronal apoptosis does not change significantly at 2–3 months of diabetes in C57BL/6J strain, despite other evidences of retinal vascular pathology [34].

### ASM-Deficiency in BM Improves CAC Release and Homing to Retinal Vasculature

Apart from giving rise to all blood cells, HSC in the BM also differentiate into reparative CACs, which circulate in blood and home to areas of injury to mediate vascular repair [35]. Accumulating evidence suggests that BM neuropathy affects CAC proliferation, release, and migration in diabetes [10]. We observed impaired release of CACs, leading to higher number of CACs in BM of 2 month-diabetic WT chimeras (Fig. 2A) as well as lower numbers of diabetic CACs in circulation (Fig. 2B), which was prevented in diabetic ASM$^{-/-}$ BM chimeras.

To directly assess effect of ASM inhibition in CACs on in vivo homing capacity, we injected gfp[+]-expressing CACs treated with ASM-siRNA into vitreous of 8–9 month diabetic WT mice. Approximately fivefold inhibition of ASM was achieved (Supporting Information Fig. S2). Seven days postinjection, retinas were analyzed for colocalization of retinal vasculature with gfp^{+} progenitor cells. When healthy CACs were injected into the vitreous of diabetic mice, we observed their participation in vessel repair as demonstrated by yellow color, due to colocalization of green (gfp[+] CACs) and red (retinal vasculature staining) (Fig. 2C, left panel). Diabetic CACs lose this ability and do not migrate to the site of injury (Fig. 2C, middle panel); however, diabetic CACs after ASM inhibition participated in repair to similar levels as control CACs (Fig. 2C, right panel). These data indicate that specific inhibition of ASM in CACs restores their reparative capacity in a DR model.

## ASM Inhibition Reduces Ceramide Levels in CACs and BM Cells

To assess effect of ASM deficiency on sphingolipid metabolism in BM cells, we characterized SM and ceramide species using mass spectra from lipid extracts of WT and ASM^{−/−} BM cells and CACs. A dramatic increase in SM and concomitant decrease in ceramide was observed in ASM^{−/−} BM cells and CACs compared to WT (Fig. 3A, 3B, Table 2; Supporting Information Fig. S3).

Ceramide metabolites such as glucosylceramides, sphingosine, and S1P play important roles in insulin resistance, as well as cellular proliferation and migration [22, 36]. We examined the effect of ASM deficiency on ceramide metabolites in ASM^{−/−} BM cells and CACs compared to WT. While we observed a decrease in some hexosylceramide species, we did not observe any significant differences in sphingosine or S1P levels (Table 2).

We next determined the effect of diabetes on CACs ceramide levels in WT and ASM^{−/−} BMT mice. As limited amount of material isolated from these stably engrafted long term diabetic mice does not allow for detailed mass spectrometry analysis, we used an alternative immunohistochemistry method using anti-ceramide antibodies. Approximately 50% increase in ceramide level was observed in diabetic CACs. In contrast, ASM^{−/−} BMT prevented this increase in ceramide levels in diabetic mice (Fig. 3C).

## Ceramide Levels Alter Membrane Viscosity of Synthetic Vesicles and Progenitor Cells

Membrane deformability can be modulated by membrane lipid content [35, 37]. We first determined the effect of ceramide on membrane viscosity of artificial vesicles by replacing 50% of SM with equal length ceramide in model lipid bilayers. To measure membrane viscosity, we labeled synthetic vesicles with a fluorescent probe, perylene (Fig. 4A)— nonpolar polycyclic aromatic hydrocarbon that incorporates selectively into bilayer nonpolar region with well-characterized rotational diffusion behavior [28]. Viscosity of extruded synthetic vesicles was quantitated by rotational diffusion of perylene. We observed that replacing sphingomyelin with ceramide in synthetic vesicles caused a significant increase in viscosity of membranes (Fig. 4A). We then determined the effect of ceramide on membrane viscosity of CACs. Membrane viscosity decreases significantly in ASM^{−/−} CACs, indicating that loss of ASM prevents cell membrane rigidity in CACs (Fig. 4B).

### ASM$^{-/-}$ BM Transfer Corrects Diabetes-Induced Deficiency in CAC Migration

Because migration of CACs is central to their function as reparative cells, we sought to understand if change in membrane rigidity due to ceramide is associated with diabetes-induced reduction in CAC motility. Increased membrane rigidity in CACs isolated from mice at 3 months of diabetes correlates with their reduced migration ability. However, membrane rigidity was normalized in diabetic CACs from ASM$^{-/-}$ BM chimeras, which further correlated with improved migration ability (Fig. 4C, 4D).

### Retinal Vascular Damage Is Prevented in Diabetic ASM$^{-/-}$ BM Chimeric Mice

We examined whether the combination of improved CAC migration and reduced activation of BM-derived inflammatory cells could prevent retinal vascular degeneration in diabetic ASM$^{-/-}$ BM chimeras. We observed increased vascular permeability as assessed by leakage of FITC-albumin compared to control chimeras, and this increase was prevented in diabetic ASM$^{-/-}$ BM chimeras (Fig. 5A).

Acellular capillaries are a histopathological hallmark of DR. We observed a significant increase in acellular capillaries in diabetic as compared to control WT BM chimeric mice (Fig. 5B). This increase was prevented in diabetic ASM$^{-/-}$ BM chimeras, supporting the hypothesis that ASM inhibition selectively in the BM is sufficient to protect from diabetes-induced retinal vascular pathology.

## Discussion

Landmark clinical trials, DCCT and ACCORD Eye demonstrated that control of hyperglycemia and dyslipidemia is required to achieve maximal protection from DR [18, 19]. Although hyperglycemia-associated damage has been studied in detail, few studies addressed the effect of dyslipidemia in DR. Dyslipidemia is a complex metabolic dysregulation of multiple lipid classes including triglycerides, cholesterol, esterified and non-esterified fatty acids, and sphingolipids.

Previous studies by others and us indicated that dysregulation of sphingolipid metabolism, with upregulation of ASM and higher hexosyl ceramide production plays an important role in diabetic dyslipidemia-induced retinal damage [20, 22, 23]. However, whole-body ASM deficiency leads to retinal dysfunction and neurodegeneration in ASM$^{-/-}$ mice [38, 39]. A recent study by Dannhausen et al. demonstrates activation of microglia and loss of retinal function in ASM$^{-/-}$ mice [38].

In addition to previously reported direct retinal effects, ASM upregulation could also affect the BM niche, disturbing the balance between proinflammatory and reparative BM cell populations. This affords us an opportunity to inhibit ASM only in the BM cells, thus avoiding the unwanted neurodegenerative effects due to systemic ASM inhibition. To achieve selective BM inhibition in this study, we have generated chimeric mice by ASM$^{-/-}$ → WT or WT → WT BM transplantation. BM transplantation ensures that all the cells derived from the BM are ASM deficient, while ASM activity is maintained in other tissues, including retina.

Dysfunction of BM-derived CACs is a critical component of the pathogenic events associated with DR [40, 41]. Recent studies indicate that CACs isolated from diabetic patients are not effective in vascular regeneration due to impaired migration, proliferation, and differentiation [10, 12, 42]. Advanced diabetes is associated with BM neuropathy which contributes to the inability of CAC to egress the BM, enter the circulation, and home to areas of injury [43, 44]. Thus, this trapping of CACs within the BM makes these cells unavailable for vascular repair [10]. Furthermore, the migratory prowess of diabetic CACs is severely altered due to their inability to respond to hypoxia with an increase in hypoxia-inducible factor (HIF) expression or to migrate toward gradients of hypoxia regulated factors, such as VEGF-A and stromal derived factor-1 (SDF-1) [14, 45, 46]. The migratory defect of these cells is a result of reduced bioavailability of nitric oxide (NO) as well as poor deformability [14].

We have previously demonstrated that blocking upregulation of ASM in diabetic CACs leads to improved colony forming ability, indicating an improved capacity of these reparative cells to adhere and differentiate in culture [13]. Recently, ceramide metabolites such as C1P and S1P were found to upregulate SDF-1 secretion from BM stromal cells, potentially altering chemokine gradients that guide the release of progenitor cells from their BM niche [16, 47, 48]. In our study, we demonstrate that increased ceramide levels alters membrane fluidity of diabetic CACs leading to impaired CAC release from the BM and reduced migration to areas of retinal vascular injury in a mouse model of DR.

In addition to reparative CAC dysfunction, diabetes affects BM-derived inflammatory myelomonocytic cells, which circulate in blood and contribute to diabetes-associated inflammation. Previous studies showed that diabetes causes accumulation of inflammatory monocytes in the retina [7, 11]. Proinflammatory BM-derived cells, like neutrophils and monocytes, were recently demonstrated to play important roles in retinal endothelial cell death and capillary degeneration in diabetes [7]. However, the exact contribution of BM-derived microglia to retinal damage during diabetes remains unclear. During embryonic development, resident tissue microglia are known to develop from a yolk sac and do not have myeloid origin [49]. Several studies demonstrated that in normal tissue, microglial regeneration occurs from tissue-specific microglial progenitors [50]. This balance could shift toward myeloid cells with ageing, inflammation, or tissue damage [5, 9, 31]. We observed Iba$^+$ gfp$^+$ cells in control and diabetic retinas; however, Iba$^+$ gfp$^+$ cells in control retinas had branched resting phenotype compared to clearly activated amoeboid phenotype in diabetic retinas, indicating that diabetes-induced damage promotes myeloid-derived microglial activation. Furthermore, our data demonstrate that inhibition of ASM in BM prevents activation of these microglia-like cells. Reduced activation of BM-derived microglia may contribute to normalizing levels of proinflammatory cytokines and growth factors in retinas of diabetic ASM$^{-/-}$ BM chimeras.

In this study, we demonstrate that the combination of improved CAC migration and reduced activation of BM-derived inflammatory cells in ASM$^{-/-}$ BM chimeras prevents diabetes-induced retinal vascular degeneration. Vascular degeneration characterized by increase in number of acellular capillaries is typically determined after 6 months of diabetes; however, BM transplantation and stable engraftment before the induction of diabetes resulted in older

age of mice at the end of the experiment (9–11 months old). Older age likely contributed to the high numbers of acellular capillaries that we observed at 3–5 months of diabetes (Fig. 5B).

ASM activation and ceramide production can alter cell fate through a variety of mechanisms. ASM activation has been associated with increased cytokine release in the resident microglia of the retina [51]. Ceramide may serve as a second messenger in initiating apoptosis of endothelial cells, while reduction of ceramide levels by inhibiting ASM has been demonstrated to prevent endothelial cell death, leading to reduced capillary apoptosis in tumor microenvironments [52, 53]. Previously, we showed that inhibition of ASM by dietary supplementation of docosahexaenoic acid or by genetic manipulation prevents retinal vascular degeneration associated with diabetes [13, 20, 25]. However, as retinal effects of $ASM^{-/-}$ are also associated with neurodegeneration, in this study we wanted to separate the BM and retinal/vascular effects of $ASM^{-/-}$. The retina and vasculature of the chimeric animals in this study were from the WT host, only the BM was from the $ASM^{-/-}$ mice. Thus, although in the whole body $ASM^{-/-}$ model endothelial cell death is inhibited, the model we used does not directly affect endothelial ASM expression levels and the effects we observed were mediated by changes in BM progenitors.

In this study, we explore the role of ceramide as a structural membrane component contributing to membrane fluidity. Ceramide has a tendency to self-associate, forming ceramide-enriched platforms in the cell membrane [54]. These altered membrane microdomains have been demonstrated to enhance inflammatory signal transduction by facilitating receptor clustering, thereby promoting survival and immune activation of a variety of immune cells including monocytes [54–56]. Here, we further explore the concept that altered membrane fluidity of diabetic CACs leads to their impaired release and migration, making them unavailable for vascular repair. These roles of ceramide are not conflicting—these effects are likely happening simultaneously with decreased membrane fluidity, endothelial cell apoptosis, and proinflammatory pathways contributing to pathogenesis of DR.

Various sphingolipids, such as glycosphingolipids, sphingosine, and S1P have been shown to play a role in development of DR [20–22, 24]. Ceramide can be metabolized into S1P, which has proliferation, migration, and prosurvival effects [35]. Elevated levels of S1P are shown to contribute to retinal vascular pathology in animal models of diabetes [21, 24]. However, we did not observe any changes in sphingosine or S1P levels in $ASM^{-/-}$ mouse BM cells or CACs, indicating that although these bioactive lipids may be involved in other aspects of diabetes-induced damage, they cannot explain the correction of deficient migration or normalization of proinflammatory pathways observed in $ASM^{-/-}$ BMT mice in this study.

Apart from the important role of ceramide in inflammatory responses, there is also a well-established literature indicating that presence of ceramide and cholesterol in a lipid bilayer causes a change in "viscosity" of membranes [54, 57, 58]. We have previously demonstrated that diabetes is associated with reduced deformability of human CACs, this reduced deformability is associated with decreased migratory prowess [14] and that ASM activation leads to increased short-chain ceramide levels in diabetic CACs [13]. In this study, we show

that increased levels of membrane ceramide due to ASM activation in diabetes are associated with increased membrane rigidity, impaired migration and extravasation capacity of CACs, which in turn prevents effective homing from BM to sites of vascular injury.

Taken together, these data suggest that modifying membrane lipid composition of diabetic BM-derived cells may be beneficial for preventing retinal vascular degeneration. Conceivably, measure of membrane rigidity could be used in the clinic as a mechanical biomarker to gain evidence of ongoing biological stress and tissue damage due to diabetic dyslipidemia. Furthermore, correction of membrane rigidity can be explored as a potential treatment strategy to improve migration and repair function of CACs in diabetic patients. Intravenous infusion of autologous CACs corrected for membrane rigidity ex vivo could be used as a therapeutic strategy to enhance repair in vivo [15]. Cell therapy is ideal for treatment of diabetic patients as microvascular disease does not lend itself to revascularization procedures such as stents and angioplasty but is amenable to cell therapy. The interest in cell therapy is apparent as CD34+ cells are the most commonly used cells for human regenerative studies. There are 388 trials using CD34+ cells listed on Clinical Trials.gov, including one trial using these cells for retinal vascular repair in diabetes (NCT01736059).

## Conclusion

In conclusion, we demonstrated that pathological activation of ASM in BM-derived cells plays a crucial role in diabetes-induced retinal vascular degeneration by activating microglia-like BM-derived cells that infiltrate the retina, and preventing efficient retinal vascular repair by reparative CACs. Our studies provide novel insights into the highly complex mechanisms that lead to retinal vascular degeneration in diabetes and suggest that strategies targeting normalization of ASM in BM-derived cell populations, thereby controlling the balance between reparative and proinflammatory cells could represent a viable cell therapy option to enhance available DR treatments.

## Supplementary Material

Refer to Web version on PubMed Central for supplementary material.

## Acknowledgments

## References

1. Antonetti DA, Klein R, Gardner TW. Diabetic retinopathy. N Engl J Med. 2012; 366:1227–1239. [PubMed: 22455417]

2. Kern TS. Contributions of inflammatory processes to the development of the early stages of diabetic retinopathy. Exp Diabetes Res. 2007; 2007:95103. [PubMed: 18274606]

3. Mohr S. Potential new strategies to prevent the development of diabetic retinopathy. Expert Opin Investig Drugs. 2004; 13:189–198.

4. Busik JV, Mohr S, Grant MB. Hyperglycemia-induced reactive oxygen species toxicity to endothelial cells is dependent on paracrine mediators. Diabetes. 2008; 57:1952–1965. [PubMed: 18420487]

5. Abcouwer SF. Angiogenic factors and cytokines in diabetic retinopathy. J Clin Cell Immunol. 2013; (suppl 1)

6. Li G, Veenstra AA, Talahalli RR, et al. Marrow-derived cells regulate the development of early diabetic retinopathy and tactile allodynia in mice. Diabetes. 2012; 61:3294–3303. [PubMed: 22923475]

7. Schroder S, Palinski W, Schmid-Schonbein GW. Activated monocytes and granulocytes, capillary nonperfusion, and neovascularization in diabetic retinopathy. Am J Pathol. 1991; 139:81–100. [PubMed: 1713023]

8. Hinze A, Stolzing A. Differentiation of mouse bone marrow derived stem cells toward microglia-like cells. BMC Cell Biol. 2011; 12:35. [PubMed: 21854582]

9. Soulet D, Rivest S. Bone-marrow-derived microglia: Myth or reality? Curr Opin Pharmacol. 2008; 8:508–518. [PubMed: 18487084]

10. Busik JV, Tikhonenko M, Bhatwadekar A, et al. Diabetic retinopathy is associated with bone marrow neuropathy and a depressed peripheral clock. J Exp Med. 2009; 206:2897–2906. [PubMed: 19934019]

11. Hazra S, Jarajapu YP, Stepps V, et al. Long-term type 1 diabetes influences haematopoietic stem cells by reducing vascular repair potential and increasing inflammatory monocyte generation in a murine model. Diabetologia. 2013; 56:644–653. [PubMed: 23192694]

12. Loomans CJ, de Koning EJ, Staal FJ, et al. Endothelial progenitor cell dysfunction: A novel concept in the pathogenesis of vascular complications of type 1 diabetes. Diabetes. 2004; 53:195–199. [PubMed: 14693715]

13. Tikhonenko M, Lydic TA, Opreanu M, et al. N-3 polyunsaturated fatty acids prevent diabetic retinopathy by inhibition of retinal vascular damage and enhanced endothelial progenitor cell reparative function. PLoS One. 2013; 8:e55177. [PubMed: 23383097]

14. Segal MS, Shah R, Afzal A, et al. Nitric oxide cytoskeletal-induced alterations reverse the endothelial progenitor cell migratory defect associated with diabetes. Diabetes. 2006; 55:102–109. [PubMed: 16380482]

15. Shaw LC, Neu MB, Grant MB. Cell-based therapies for diabetic retinopathy. Curr Diabetes Rep. 2011; 11:265–274.

16. Kim C, Schneider G, Abdel-Latif A, et al. Ceramide-1-phosphate regulates migration of multipotent stromal cells (MSCs) and endothelial progenitor cells (EPCs)—Implications for tissue regeneration. Stem Cells. 2013; 31:500–510. [PubMed: 23193025]

17. Tongers J, Roncalli JG, Losordo DW. Therapeutic angiogenesis for critical limb ischemia: Microvascular therapies coming of age. Circulation. 2008; 118:9–16. [PubMed: 18591450]

18. Lyons TJ, Jenkins AJ, Zheng D, et al. Diabetic retinopathy and serum lipoprotein subclasses in the DCCT/EDIC cohort. Invest Ophthalmol Vis Sci. 2004; 45:910–918. [PubMed: 14985310]

19. Chew EY, Ambrosius WT, Davis MD, et al. Effects of medical therapies on retinopathy progression in type 2 diabetes. New Engl J Med. 2010; 363:233–244. [PubMed: 20587587]

20. Opreanu M, Tikhonenko M, Bozack S, et al. The unconventional role of acid sphingomyelinase in regulation of retinal microangiopathy in diabetic human and animal models. Diabetes. 2011; 60:2370–2378. [PubMed: 21771974]

21. Fox TE, Bewley MC, Unrath KA, et al. Circulating sphingolipid biomarkers in models of type 1 diabetes. J Lipid Res. 2011; 52:509–517. [PubMed: 21068007]

22. Fox TE, Han X, Kelly S, et al. Diabetes alters sphingolipid metabolism in the retina: A potential mechanism of cell death in diabetic retinopathy. Diabetes. 2006; 55:3573–3580. [PubMed: 17130506]

Author Manuscript Author Manuscript Author Manuscript Author Manuscript

23. Busik JV, Esselman WJ, Reid GE. Examining the role of lipid mediators in diabetic retinopathy. Clin Lipidol. 2012; 7:661–675. [PubMed: 23646066]

24. Maines LW, French KJ, Wolpert EB, et al. Pharmacologic manipulation of sphingosine kinase in retinal endothelial cells: Implications for angiogenic ocular diseases. Invest Ophthalmol Vis Sci. 2006; 47:5022–5031. [PubMed: 17065523]

25. Opreanu M, Lydic TA, Reid GE, et al. Inhibition of cytokine signaling in human retinal endothelial cells through downregulation of sphingomyelinases by docosahexaenoic acid. Invest Ophthalmol Vis Sci. 2010; 51:3253–3263. [PubMed: 20071681]

26. Kielczewski JL, Calzi SL, Shaw LC, et al. Free Insulin-like growth factor binding protein-3 (IGFBP-3) reduces retinal vascular permeability in association with a reduction of acid sphingomyelinase (ASMase). Invest Ophthalmol Vis Sci. 2011; 52:8278–8286. [PubMed: 21931131]

27. Medina RJ, O'Neill CL, O'Doherty TM, et al. Myeloid angiogenic cells act as alternative M2 macrophages and modulate angiogenesis through interleukin-8. Mol Med. 2011; 17:1045–1055. [PubMed: 21670847]

28. Lapinski MM, Blanchard GJ. Interrogating the role of liposome size in mediating the dynamics of a chromophore in the acyl chain region of a phospholipid bilayer. Chem Phys Lipids. 2008; 153:130–137. [PubMed: 18396153]

29. Lydic TA, Busik JV, Reid GE. A monophasic extraction strategy for the simultaneous lipidome analysis of polar and nonpolar retina lipids. J Lipid Res. 2014; 55:1797–1809. [PubMed: 24879804]

30. Rungger-Brandle E, Dosso AA, Leuenberger PM. Glial reactivity, an early feature of diabetic retinopathy. Invest Ophthalmol Vis Sci. 2000; 41:1971–1980. [PubMed: 10845624]

31. Zeng XX, Ng YK, Ling EA. Neuronal and microglial response in the retina of streptozotocin-induced diabetic rats. Vis Neurosci. 2000; 17:463–471. [PubMed: 10910112]

32. Barber AJ, Antonetti DA, Kern TS, et al. The Ins2Akita mouse as a model of early retinal complications in diabetes. Invest Ophthalmol Vis Sci. 2005; 46:2210–2218. [PubMed: 15914643]

33. Martin PM, Roon P, Van Ells TK, et al. Death of retinal neurons in streptozotocin-induced diabetic mice. Invest Ophthalmol Vis Sci. 2004; 45:3330–3336. [PubMed: 15326158]

34. Feit-Leichman RA, Kinouchi R, Takeda M, et al. Vascular damage in a mouse model of diabetic retinopathy: Relation to neuronal and glial changes. Invest Ophthalmol Vis Sci. 2005; 46:4281–4287. [PubMed: 16249509]

35. Catapano ER, Arriaga LR, Espinosa G, et al. Solid character of membrane ceramides: A surface rheology study of their mixtures with sphingomyelin. Biophys J. 2011; 101:2721–2730. [PubMed: 22261061]

36. Hla T. Physiological and pathological actions of sphingosine 1-phosphate. Semin Cell Dev Biol. 2004; 15:513–520. [PubMed: 15271296]

37. Boulgaropoulos B, Rappolt M, Sartori B, et al. Lipid sorting by ceramide and the consequences for membrane proteins. Biophys J. 2012; 102:2031–2038. [PubMed: 22824266]

38. Dannhausen K, Karlstetter M, Caramoy A, et al. Acid sphingomyelinase (aSMase) deficiency leads to abnormal microglia behavior and disturbed retinal function. Biochem Biophys Res Commun. 2015; 464:434–440. [PubMed: 26129774]

39. Horinouchi K, Erlich S, Perl DP, et al. Acid sphingomyelinase deficient mice: A model of types A and B Niemann-Pick disease. Nat Genet. 1995; 10:288–293. [PubMed: 7670466]

40. Tang J, Kern TS. Inflammation in diabetic retinopathy. Prog Retin Eye Res. 2011; 30:343–358. [PubMed: 21635964]

41. Marchetti V, Yanes O, Aguilar E, et al. Differential macrophage polarization promotes tissue remodeling and repair in a model of ischemic retinopathy. Sci Rep. 2011; 1:76. [PubMed: 22355595]

42. Caballero S, Sengupta N, Afzal A, et al. Ischemic vascular damage can be repaired by healthy, but not diabetic, endothelial progenitor cells. Diabetes. 2007; 56:960–967. [PubMed: 17395742]

43. Said G. Focal and multifocal diabetic neuropathies. Arq neuro-psiquiatr. 2007; 65:1272–1278.

44. Hu P, Thinschmidt JS, Yan Y, et al. CNS inflammation and bone marrow neuropathy in type 1 diabetes. Am J Pathol. 2013; 183:1608–1620. [PubMed: 24160325]

45. Li Calzi S, Purich DL, Chang KH, et al. Carbon monoxide and nitric oxide mediate cytoskeletal reorganization in microvascular cells via vasodilator-stimulated phosphoprotein phosphorylation: Evidence for blunted responsiveness in diabetes. Diabetes. 2008; 57:2488–2494. [PubMed: 18559661]

46. Jarajapu YP, Hazra S, Segal M, et al. Vasoreparative dysfunction of CD34 + cells in diabetic individuals involves hypoxic desensitization and impaired autocrine/paracrine mechanisms. PLoS One. 2014; 9:e93965. [PubMed: 24713821]

47. Golan K, Vagima Y, Ludin A, et al. S1P promotes murine progenitor cell egress and mobilization via S1P1-mediated ROS signaling and SDF-1 release. Blood. 2012; 119:2478–2488. [PubMed: 22279055]

48. Kim CH, Wu W, Wysoczynski M, et al. Conditioning for hematopoietic transplantation activates the complement cascade and induces a proteolytic environment in bone marrow: A novel role for bioactive lipids and soluble C5b-C9 as homing factors. Leukemia. 2012; 26:106–116. [PubMed: 21769103]

49. Ginhoux F, Lim S, Hoeffel G, et al. Origin and differentiation of microglia. Front Cell Neurosci. 2013; 7:45. [PubMed: 23616747]

50. Ajami B, Bennett JL, Krieger C, et al. Local self-renewal can sustain CNS microglia maintenance and function throughout adult life. Nat Neurosci. 2007; 10:1538–1543. [PubMed: 18026097]

51. Bianco F, Perrotta C, Novellino L, et al. Acid sphingomyelinase activity triggers microparticle release from glial cells. EMBO J. 2009; 28:1043–1054. [PubMed: 19300439]

52. Garcia-Barros M, Paris F, Cordon-Cardo C, et al. Tumor response to radiotherapy regulated by endothelial cell apoptosis. Science. 2003; 300:1155–1159. [PubMed: 12750523]

53. Kolesnick R, Fuks Z. Radiation and ceramide-induced apoptosis. Oncogene. 2003; 22:5897–5906. [PubMed: 12947396]

54. Stancevic B, Kolesnick R. Ceramide-rich platforms in transmembrane signaling. FEBS Lett. 2010; 584:1728–1740. [PubMed: 20178791]

55. Grassme H, Riethmuller J, Gulbins E. Biological aspects of ceramide-enriched membrane domains. Prog Lipid Res. 2007; 46:161–170. [PubMed: 17490747]

56. Pfeiffer A, Bottcher A, Orso E, et al. Lipopolysaccharide and ceramide docking to CD14 provokes ligand-specific receptor clustering in rafts. Eur J Immunol. 2001; 31:3153–3164. [PubMed: 11745332]

57. Goni FM, Alonso A. Biophysics of sphingolipids I. Membrane properties of sphingosine, ceramides and other simple sphingolipids. Biochim Biophys Acta. 2006; 1758:1902–1921. [PubMed: 17070498]

58. Song J, Waugh RE. Bending rigidity of SOPC membranes containing cholesterol. Biophys J. 1993; 64:1967–1970. [PubMed: 8369417]

## Significance Statement

Diabetic retinopathy (DR) remains a challenge in clinical ophthalmology since current approaches for treatment are highly invasive and do not fully prevent or reverse pathology. Previous studies have demonstrated that bone marrow dysfunction in diabetes critically contributes to retinal vascular degeneration. We explore a novel concept that altered sphingolipid metabolism in the bone marrow plays a crucial role in diabetes-induced retinal vascular degeneration by activating inflammatory cells that infiltrate the retina and preventing efficient retinal vascular repair by reparative cells. Our studies identify for the first time, that modulation of acid sphingomyelinase to control ceramide content in bone marrow cells, including therapeutic progenitor cells membranes can be a highly effective therapeutic target for correcting vascular degeneration associated with diabetic retinopathy.
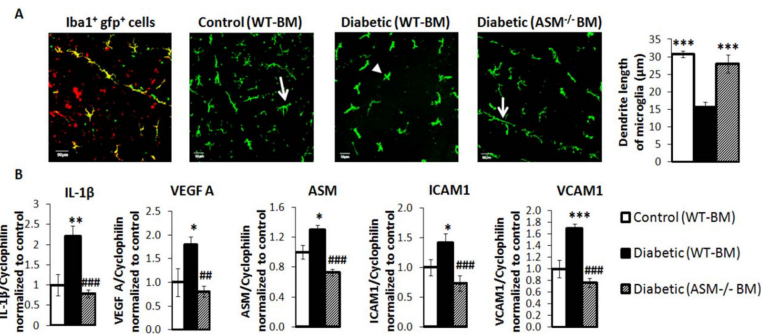
**Figure 1.**
ASM deficiency in BM prevents inflammation in diabetic retina. **(A)**: Microglial marker Iba-1$^+$ staining (red) with gfp$^+$ (green) cells, showing colocalization (yellow) in retina. Control retinas show gfp$^+$ microglia with highly ramified phenotype (white arrow). Diabetic retinas show gfp$^+$ microglia with retracted processes (white arrowhead). Diabetic retinas from ASM$^{-/-}$ BM chimeric mice show ramified phenotype (white arrow). Quantification of dendritic length of microglia is shown on the right. $n$=8 per group. ***, $p$<.001 relative to diabetic. Scale bar=50 μM. Duration of diabetes was 3 months. **(B)**: Quantitative polymerase chain reaction for relative mRNA levels of indicated genes in diabetic retinas relative to controls. Duration of diabetes was 2 months. $n$=7–10 per group. *, $p$<.05; **, $p$<.01; ***, $p$<.001 relative to control. ##, $p$<.01; ###, $p$<.001 relative to diabetic. Data are expressed as means ± SEM for all. Abbreviations: ASM, acid sphingomyelinase; BM, bone marrow; IL-1β, interleukin-1β; VEGF, vascular endothelial growth factor; ICAM-1, intercellular adhesion molecule-1; VCAM-1, vascular cell adhesion molecule-1; WT, wild-type.
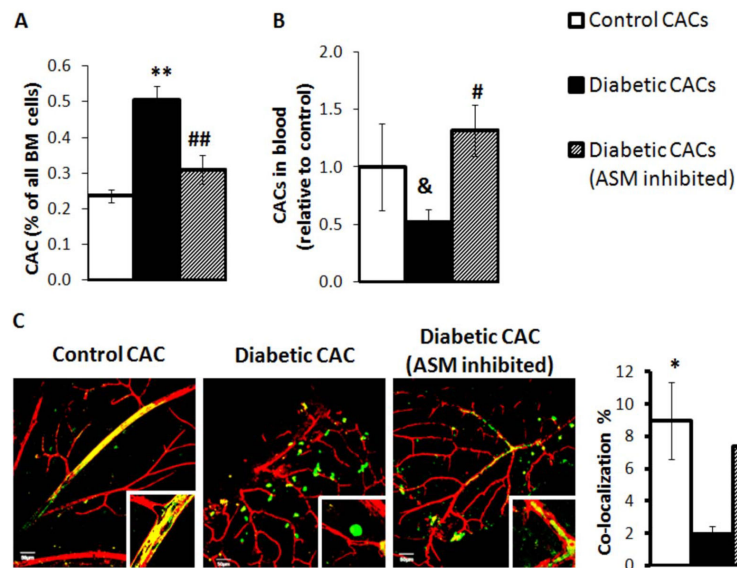
**Figure 2.**

ASM inhibition improves CAC release and incorporation into retinal vasculature. **(A)**: Percentages of CACs in BM of 2 months diabetic wild-type (WT) chimeric mice is increased compared to nondiabetic chimeras, and this is prevented in diabetic ASM$^{-/-}$ BM chimeras. $n$=4–8 per group, \*\*, $p<.01$ relative to control; $^{\#\#}$, $p<.01$ relative to diabetic. **(B)**: Percentages of CACs in blood of 2 months diabetic WT chimeric mice is decreased compared to nondiabetic chimeras, and this is prevented in diabetic ASM$^{-/-}$ BM chimeras. $n$=4–8 per group, $^{\&}$, $p$=0.07 relative to control, $^{\#}$, $p<.01$ relative to diabetic. **(C)**: Diabetic animals received intravitreal injections of control (left), diabetic (middle), or diabetic CACs treated with siRNA for ASM (right). CACs (green) were isolated from *gfp*$^{+}$ mice, retinal vasculature was stained with anticollagen IV antibody (red), and colocalization (yellow) indicates vascular association. Diabetic CACs show reduced colocalization with vasculature (middle), while ASM inhibition improves vascular association of diabetic CACs (right). Quantification of colocalization (yellow) is shown on far right. Duration of diabetes was 8–9 months. \* $p<.05$ relative to diabetic. Data are expressed as means±SEM. Scale bars=50 μM. Abbreviations: ASM, acid sphingomyelinase; BM, bone marrow; CAC, circulating angiogenic cell.
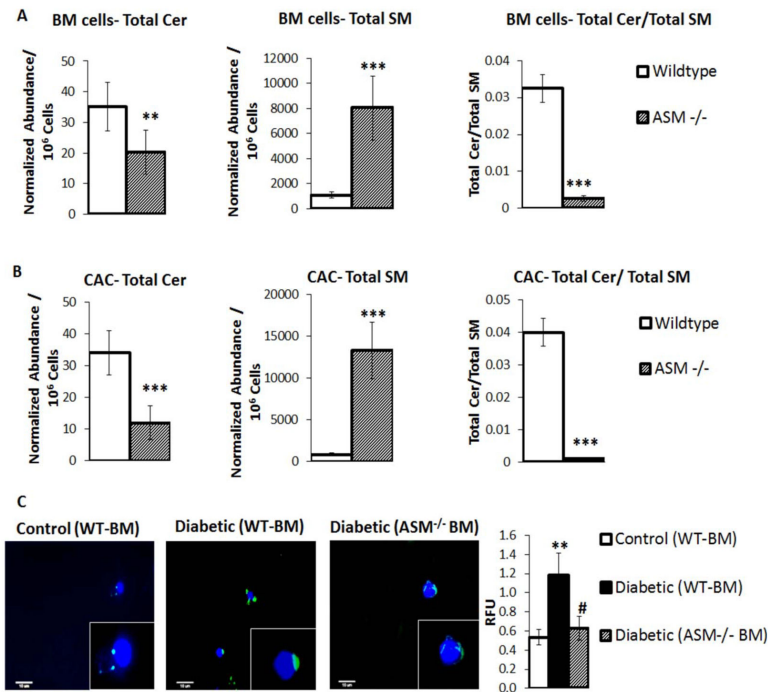
**Figure 3.**
Effect of ASM inhibition on sphingolipid metabolism in BM cells and CACs. Total ceramide and ratio of total ceramide to total SM were significantly decreased, and total SM significantly increased in ASM$^{-/-}$ BM cells **(A)** and CACs **(B)**. $n$=6 per group, **, $p$<.01; ***, $p$<.001. Data are expressed as means±SD. **(C)**: Immunofluorescence using anticeramide antibody (green) demonstrates that diabetic CACs from WT BM chimeras (middle) have increased ceramide levels compared to control CACs (left). This increase is prevented in diabetic CACs from ASM$^{-/-}$ BM chimeras (right). Scale bar=10 μM. Quantification of green fluorescence relative to DAPI nuclear stain is shown on far right. Duration of diabetes was 3 months. Data are expressed as means±SEM. $n$=4–5 per group. **, $p$<.01 relative to control; #, $p$<0.05 relative to diabetic. Abbreviations: BM, bone marrow; CAC, circulating angiogenic cell; SM, sphingomyelin; RFU, relative fluorescence units; WT, wild type.
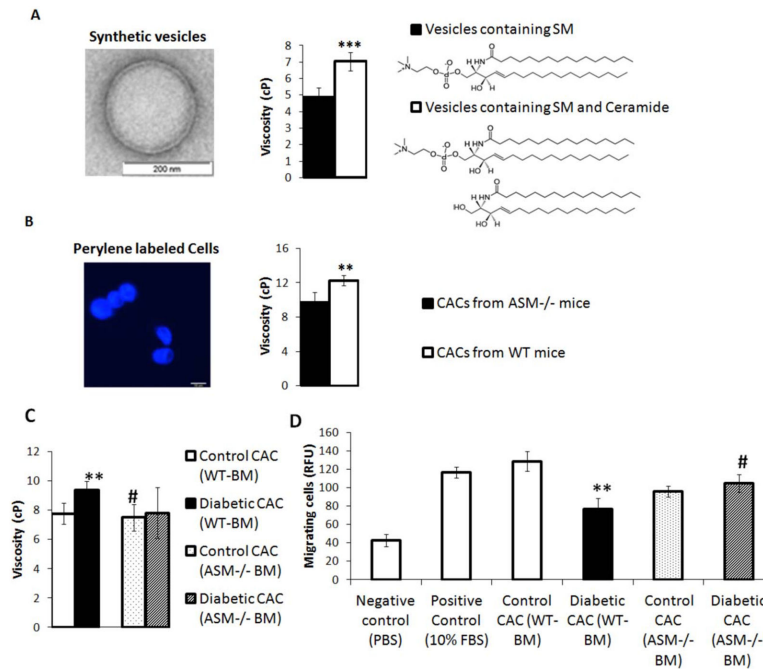
**Figure 4.**
Change in ceramide and ASM levels alter membrane viscosity of diabetic CACs. (**A**): Replacing SM with ceramide increased viscosity of synthetic membranes. ***, $p<.001$, $n=5$ per group. On Left: Extruded synthetic vesicle by electron microscopy. Data are expressed as means±SD. (**B**): CACs isolated from ASM$^{-/-}$ mice have decreased membrane viscosity compared to CACs from WT mice. $n=4–5$ per group, **, $p<.01$ relative to control. Data are expressed as means±SD. On left: Cells labeled with fluorescent probe, perylene. (**C**): Increase in membrane viscosity observed in diabetic CACs from WT chimeras was normalized in 3 months diabetic CACs from ASM$^{-/-}$ BM chimeras. Data are expressed as means±SD. $n=4–5$ per group. **, $p<.01$ relative to control; #, $p<.05$ relative to diabetic. (**D**): Migration toward SDF-1 is improved in diabetic CACs isolated from ASM$^{-/-}$ BM chimeras compared to diabetic CACs from WT chimeras. Data are expressed as means±SEM. $n=5–7$ per group, **, $p<.01$ relative to control. #, $p<.05$ relative to diabetic. Duration of diabetes was 3 months. Abbreviations: ASM, acid sphingomyelinase; BM, bone marrow; CAC, circulating angiogenic cell; FBS, fetal bovine serum; PBS, phosphate buffered saline; SM, sphingomyelin; WT, wild type.
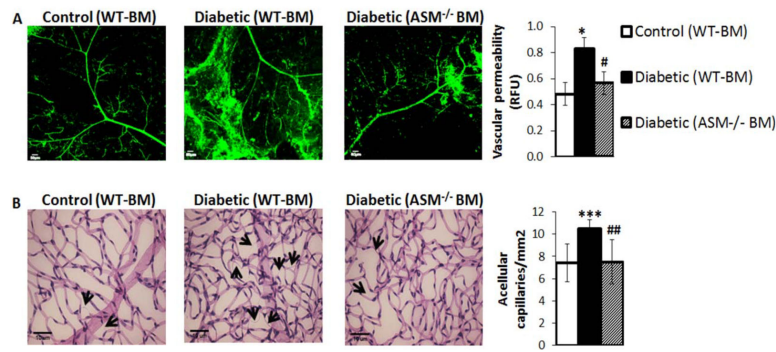
**Figure 5.**

Prevention of retinal vascular damage in diabetic ASM$^{-/-}$ BM chimeric mice. **(A)**: Diabetic retinas (2 months duration) have increased vascular permeability compared to control as demonstrated by high retinal fluorescence intensity for FITC-albumin (middle). The increase is prevented in diabetic retinas from ASM$^{-/-}$ BM chimeric mice (right). Quantification of retinal fluorescence intensity for FITC-albumin is shown on far right. $n$=10–12 per group. Data are expressed as means±SEM. *, $p$<.05 relative to control and $^\#$, $p$=0.08 relative to diabetic. Scale bar=50 μM. **(B)**: Increase in number of acellular capillaries (black arrows) in 3–5 months diabetic retina (middle) is prevented in ASM$^{-/-}$ BM chimeras (right). Quantification of acellular capillaries is shown on far right. $n$=10–14 per group. Data are expressed as means±SD. ***, $p$<.001 relative to control and $^{\#\#}$, $p$<.01 relative to diabetic. Scale bar=10 μM. Abbreviations: ASM, acid sphingomyelinase; BM, bone marrow; RFU, relative fluorescence units; WT, wild type.

**Table 1**

Average body weights and nonfasting blood glucose levels of control and diabetic mice with WT or ASM$^{-/-}$ bone marrow transplantation

| Duration of diabetes (weeks) | Treatment group | Blood glucose (mg/dL) | Weight (g) |
|---|---|---|---|
| 2 | Control (WT bone marrow) | 134±6.9 | 26±0.6 |
| 2 | Diabetic (WT bone marrow) | 361±19.3[*] | 21.2±0.5[*] |
| 2 | Diabetic (ASM$^{-/-}$ bone marrow) | 418±21.0[*] | 22.6±0.7[†] |
| 8 | Control (WT bone marrow) | 140±8.9 | 26.2±0.6 |
| 8 | Diabetic (WT bone marrow) | 427±46.6[*] | 19.4±0.3[*] |
| 8 | Diabetic (ASM$^{-/-}$ bone marrow) | 426±27.4[*] | 18.9±0.6[*] |

$n$=7–9, Data expressed as mean±s.e.m.

Abbreviations: ASM, acid sphingomyelinase; WT, wild type.

[*] Significantly different from age-matched control mice ($p<.001$).

[†] Significantly different from age-matched control mice ($p<.01$).

**Table 2**

Sphingolipids in wildtype and ASM$^{-/-}$ mouse CAC and bone marrow cells

| Lipid species (normalized abundance/10⁶ cells) | Mouse CACs | | | | Mouse bone marrow cells | | | |
|---|---|---|---|---|---|---|---|---|
| | Wildtype | ASM$^{-/-}$ | Difference | $p$ | Wildtype | ASM$^{-/-}$ | Difference | $P$ |
| Cer(d18:0/14:0) | 0.24 | 0.75 | | 0.280 | 0.36 | 0.32 | | 0.896 |
| Cer(d18:0/16:0) | 0.68 | 1.11 | | 0.412 | 1.13 | 0.69 | | 0.309 |
| Cer(d18:0/18:0) | 0.11 | 0.13 | | 0.829 | | | | |
| Cer(d18:0/22:0) | | | | | 0.07 | 0.04 | | 0.155 |
| Cer(d18:0/24:0) | | | | | 0.05 | 0.01 | ↓ | 0.010 |
| Cer(d18:1/14:0) | 0.06 | 0.07 | | 0.926 | | | | |
| Cer(d18:1/16:0) | 7.22 | 3.62 | ↓ | 0.002 | 6.48 | 4.18 | ↓ | 0.029 |
| Cer(d18:1/18:0) | 1.47 | 0.50 | ↓ | 0.011 | 0.48 | 0.29 | | 0.050 |
| Cer(d18:1/20:0) | 0.17 | 0.07 | | 0.102 | 0.10 | 0.06 | | 0.139 |
| Cer(d18:1/22:0) | 2.07 | 0.33 | ↓ | 7.1e − 7 | 2.68 | 1.18 | ↓ | 0.002 |
| Cer(d18:1/22:1) | | | | | 0.08 | 0.06 | | 0.576 |
| Cer(d18:1/23:0) | 0.37 | 0.03 | ↓ | 0.001 | 0.30 | 0.11 | ↓ | 0.032 |
| Cer(d18:1/24:0) | 6.00 | 1.17 | ↓ | 4.7e − 6 | 7.81 | 4.34 | ↓ | 0.009 |
| Cer(d18:1/24:1) | 10.83 | 3.27 | ↓ | 9.2e − 5 | 10.69 | 5.43 | ↓ | 0.001 |
| Cer(d18:1/24:2) | 4.81 | 0.85 | ↓ | 3.4e − 5 | 6.05 | 3.65 | ↓ | 0.011 |
| Hex-Cer(d18:1/16:0) | 2.09 | 0.54 | ↓ | 0.031 | 1.08 | 0.31 | ↓ | 0.004 |
| Hex-Cer(d18:1/18:0) | 0.43 | 0.05 | | 0.264 | 0.10 | 0.08 | | 0.732 |
| Hex-Cer(d18:1/20:0) | 0.44 | 0.13 | | 0.278 | 0.16 | 1.21 | | 0.388 |
| Hex-Cer(d18:1/22:0) | 2.42 | 1.03 | ↓ | 0.020 | 1.14 | 1.29 | | 0.759 |
| Hex-Cer(d18:1/24:0) | 5.21 | 1.62 | ↓ | 1.1e − 5 | 3.13 | 1.02 | ↓ | 0.002 |
| Hex-Cer(d18:1/24:1) | 4.70 | 2.46 | ↓ | 0.043 | 2.13 | 0.92 | ↓ | 0.010 |
| Hex-Cer(d18:1/24:2) | 1.02 | 0.39 | ↓ | 0.022 | 0.55 | 0.33 | | 0.127 |
| SM(d18:0/14:0) | 0.00 | 0.21 | ↑ | 0.039 | | | | |
| SM(d18:0/16:0) | 23.59 | 292.73 | ↑ | 2.4e − 6 | 29.30 | 181.15 | ↑ | 5.2e − 5 |
| SM(d18:0/17:0) | 0.01 | 0.91 | ↑ | 0.005 | | | | |
| SM(d18:0/18:0) | 0.83 | 30.59 | ↑ | 5.6e − 7 | 0.82 | 17.97 | ↑ | 6.3e − 5 |
| SM(d18:1/14:0) | 0.12 | 11.07 | ↑ | 4.8e − 5 | 0.10 | 6.11 | ↑ | 1.7e − 5 |
| SM(d18:1/15:0) | 1.33 | 15.97 | ↑ | 5.5e − 6 | 1.44 | 8.79 | ↑ | 0.0001 |
| SM(d18:1/16:0) | 330.12 | 3480.86 | ↑ | 5.2e − 6 | 371.04 | 2063.66 | ↑ | 5.1e − 5 |
| SM(d18:2/16:0) | 3.02 | 32.01 | ↑ | 7.2e − 6 | 2.85 | 18.02 | ↑ | 2.6e − 5 |
| SM(d18:1/17:0) | 3.09 | 24.15 | ↑ | 2.7e − 5 | 4.03 | 14.50 | ↑ | 0.002 |
| SM(d18:1/18:0) | 20.33 | 448.63 | ↑ | 2.1e − 6 | 14.57 | 252.65 | ↑ | 4.4e − 5 |
| SM(d18:1/18:1) | | | | | 0.10 | 13.23 | ↑ | 2.2e − 5 |
| SM(d18:2/18:1) | 0.43 | 23.95 | ↑ | 6.2e − 6 | 0.08 | 4.31 | ↑ | 2.8e − 8 |
| SM(d18:2/18:2) | 8.13 | 130.33 | ↑ | 0.002 | | | | |
| SM(d18:1/19:0) | 0.45 | 11.68 | ↑ | 5.7e − 6 | | | | |
| SM(d18:1/20:0) | 9.54 | 174.27 | ↑ | 2.7e − 6 | 7.23 | 100.65 | ↑ | 6.6e − 5 |
| SM(d18:1/20:1) | 0.12 | 16.21 | ↑ | 3.9e − 6 | 0.11 | 9.12 | ↑ | 5.4e − 5 |

| Lipid species (normalized abundance/$10^6$ cells) | Mouse CACs | | | | Mouse bone marrow cells | | | |
|---|---|---|---|---|---|---|---|---|
| | Wildtype | ASM$^{-/-}$ | Difference | $p$ | Wildtype | ASM$^{-/-}$ | Difference | $P$ |
| SM(d18:2/20:1) | | | | | 0.00 | 0.35 | ↑ | 2.8e − 6 |
| SM(d18:1/21:0) | 7.56 | 23.80 | ↑ | 0.002 | 9.17 | 15.63 | | 0.160 |
| SM(d18:1/22:0) | 34.48 | 969.78 | ↑ | 1.9e − 6 | 43.07 | 606.24 | ↑ | 5.07e − 5 |
| SM(d18:1/22:1) | 4.62 | 171.11 | ↑ | 3.1e − 6 | 6.35 | 99.97 | ↑ | 5.4e − 5 |
| SM(d18:2/22:1) | 2.66 | 76.66 | ↑ | 1.1e − 5 | 3.52 | 43.41 | ↑ | 8.3e − 5 |
| SM(d18:1/23:0) | 7.04 | 154.43 | ↑ | 4.2e − 6 | 9.08 | 97.85 | ↑ | 0.0002 |
| SM(d18:1/23:1) | 1.19 | 41.09 | ↑ | 6.2e − 6 | 1.37 | 23.91 | ↑ | 0.0001 |
| SM(d18:1/23:2) | | | | | 0.12 | 2.11 | ↑ | 0.004 |
| SM(d18:1/24:0) | 46.63 | 1455.81 | ↑ | 1.6e − 6 | 76.79 | 947.45 | ↑ | 3.4e − 5 |
| SM(d18:1/24:1) | 185.69 | 2727.35 | ↑ | 3.2e − 6 | 252.45 | 1704.36 | ↑ | 6.3e − 5 |
| SM(d18:1/24:2) | 163.95 | 2687.45 | ↑ | 6.7e − 6 | 249.41 | 1654.85 | ↑ | 9.9e − 5 |
| SM(d18:2/24:2) | | | | | 7.41 | 83.78 | ↑ | 3.6e − 5 |
| SM(d18:1/24:3) | 5.32 | 149.91 | ↑ | 1.4e − 5 | | | | |
| SM(d18:1/25:0) | 0.08 | 28.25 | ↑ | 4.2e − 6 | 0.30 | 17.32 | ↑ | 6.3e − 5 |
| SM(d18:1/25:1) | 0.14 | 18.10 | ↑ | 1.0e − 5 | 0.22 | 10.64 | ↑ | 0.0001 |
| SM(d18:1/25:2) | | | | | 0.05 | 3.39 | ↑ | 0.001 |
| SM(d18:1/26:0) | 0.01 | 13.64 | ↑ | 5.5e − 6 | 0.03 | 8.30 | ↑ | 8.8e − 5 |
| SM(d18:1/26:1) | 0.13 | 21.16 | ↑ | 5.9e − 6 | 0.37 | 12.57 | ↑ | 5.7e − 5 |
| SM(d18:1/26:2) | 0.50 | 37.07 | ↑ | 7.5e − 6 | 1.61 | 22.38 | ↑ | 5.5e − 5 |
| SM(d18:1/26:3) | 0.28 | 48.13 | ↑ | 0.002 | | | | |
| Sph16:0 | 5.32 | 8.65 | ↑ | 0.048 | 6.51 | 5.82 | | 0.602 |
| Sph16:0-P | 0.00 | 0.00 | | 0.061 | 0.00 | 0.01 | | 0.149 |
| Sph16:1 | 5.91 | 5.85 | | 0.946 | 6.75 | 5.05 | | 0.188 |
| Sph16:1-P | 0.00 | 0.00 | | 0.585 | 0.00 | 0.01 | | 0.439 |
| Sph18:0 | 5.65 | 8.20 | | 0.469 | 7.51 | 6.23 | | 0.636 |
| Sph18:0-P | 0.00 | 0.01 | | 0.377 | 0.00 | 0.01 | | 0.269 |
| Sph18:1 | 7.59 | 10.28 | | 0.627 | 8.59 | 6.00 | | 0.591 |
| Sph18:1-P | 0.01 | 0.00 | | 0.845 | 0.01 | 0.01 | | 0.844 |
| Sph18:2 | 19.54 | 19.68 | | 0.993 | 9.51 | 11.59 | | 0.796 |
| Sph18:2-P | 0.00 | 0.00 | | 0.653 | 0.00 | 0.00 | | 0.054 |
| Sph20:0 | 9.82 | 12.32 | | 0.454 | 10.66 | 7.48 | | 0.223 |
| Sph20:0-P | 0.00 | 0.00 | | 0.223 | | | | |
| Sph20:1 | 12.32 | 7.85 | | 0.442 | 11.26 | 4.43 | | 0.177 |
| Sph20:1-P | 0.05 | 0.00 | | 0.196 | 0.05 | 0.02 | | 0.405 |
| Sph20:2 | 0.61 | 0.59 | | 0.940 | 0.43 | 0.27 | | 0.520 |
| Sph20:2-P | 0.00 | 0.01 | | 0.488 | 0.01 | 0.00 | | 0.434 |

Arrows pointing up indicate significant increase; arrows pointing down indicate significant decrease in ASM$^{-/-}$ as compared to wildtype.

Abbreviations: ASM, acid sphingomyelinase; CAC, circulating angiogenic cells; Cer, ceramide, Hex-Cer, hexosyl ceramide; SM, sphingomyelin; sph: sphingosine; sph-P: sphingosine phosphate.